RSC Advances

PAPER

View Article Online
View Journal | View Issue

Cite this: *RSC Adv.*, 2019, **9**, 32027

Dispersed GaOOH rods loaded on the surface of $ZnBiNbO_5$ particles with enhanced photocatalytic activity toward enrofloxacin

Panqi Huang and Jingfei Luan*

A GaOOH/$ZnBiNbO_5$ composite was constructed by loading dispersed GaOOH rods on the surface of $ZnBiNbO_5$ particles and characterizations, including SEM-EDS, XRD, FT-IR spectroscopy, XPS, and UV-Vis DRS, were performed to analyze the morphology, structure and optical properties of the GaOOH/$ZnBiNbO_5$ composite. The characterization results showed that $ZnBiNbO_5$ was not destroyed by a high temperature and high pressure in the solvothermal process and that GaOOH was successfully dispersed on the surface of $ZnBiNbO_5$. Simultaneously, there was a red-shift of the absorbance edge for GaOOH/$ZnBiNbO_5$ compared with those of pure $ZnBiNbO_5$ and pure GaOOH. The band gaps of $ZnBiNbO_5$, GaOOH and GaOOH/$ZnBiNbO_5$ were calculated to be 2.96 eV, 4.76 eV and 2.93 eV, respectively. The photocatalytic activity of GaOOH/$ZnBiNbO_5$ was explored by degrading enrofloxacin under illumination. After ultraviolet light irradiation for 60 min, the removal rate of enrofloxacin with GaOOH/$ZnBiNbO_5$ as a photocatalyst was 15.11% higher than that of pure $ZnBiNbO_5$ and was 29.29% higher than that of pure GaOOH. In addition, the contribution of the free radicals in the photocatalytic process was confirmed to be $\cdot O_2^-$ > $\cdot OH$ > h^+. The construction of the GaOOH/$ZnBiNbO_5$ composite improved the performance of the single $ZnBiNbO_5$ photocatalyst and single GaOOH photocatalyst, thereby increasing their practical application potential.

Received 7th August 2019
Accepted 23rd September 2019

DOI: 10.1039/c9ra06153c

rsc.li/rsc-advances

Introduction

In recent years, veterinary drugs have been widely and commonly used to treat many animal diseases.[1–3] Antibiotics are among the most widely used veterinary drugs because antibiotics can not only treat and prevent animal diseases, but also promote animal growth and improve the nutritional value of animal foods.[4,5] Among these, enrofloxacin is a fluoroquinolone antibiotic that is the most commonly used antibacterial compound in veterinary applications.[6] The extensive use of enrofloxacin has caused serious environmental pollution mainly due to the use of contaminated livestock waste as a natural fertilizer.[7,8] In addition, since in most cases, the equipment in sewage treatment plants cannot completely treat antibiotic-like pollutants, enrofloxacin is also discharged into the environment through the wastewater of the wastewater treatment plants.[9–13] The presence of antibiotic contaminants in the environment has a negative impact on biota and can promote and spread antibiotic resistance.[14–16]

The photocatalysis technology has the advantages of environmental protection, high efficiency and low cost. The key to the photocatalytic technology is the development of highly efficient photocatalysts. According to previous reports,[17–22] many metal oxides, such as TiO_2 and ZnO_2, have been developed as photocatalysts. Because single photocatalysts have some inherent characteristics, such as photo-etching and wide band gaps, their applications are limited. It is important to improve the photocatalytic performance of photocatalysts; many methods have been proven to be effective, such as ion doping methods,[23–25] construction of heterojunctions,[26–31] and photosensitization.[32–35] Among these, the construction of composites is an active area of research in the field of photocatalysts. A composite photocatalyst concentrates the effects of single photocatalysts, which endows the composite system with higher light utilization efficiency, longer carrier life, higher photocatalytic performance and higher chemical stability.[36,37]

Several years ago, Zou *et al.*[38] reported that multiple metal oxides prepared by solid-state reactions showed good photocatalytic activity under light irradiation. In recent years, many multiple metal oxides have been prepared and reported. For example, $NiCo_2O_4$ was reported to have good photocatalytic activity for degrading MB under light irradiation.[39] In addition, in our previous studies, Gd_2YbSbO_7 and In_2YbSbO_7 with the pyrochlore-type structure were prepared by solid-state reactions and showed enhanced photocatalytic performances under light irradiation.[40] Along this line, we synthesized multiple metal oxides, such as $ZnBiNbO_5$, using the solid-state reaction method. At the same time, GaOOH was selected to construct

State Key Laboratory of Pollution Control and Resource Reuse, School of the Environment, Nanjing University, Nanjing, 210023, People's Republic of China. E-mail: jfluan@nju.edu.cn

heterojunctions with $ZnBiNbO_5$. Due to the low potential of the valence band of GaOOH, it has high oxidizing power for various photocatalytic reactions.[41] Additionally, twisted octahedral GaO_6 forms the unit cell of GaOOH, which can generate a strong dipole moment and improve the separation of photogenerated electrons and photogenerated holes.[42]

Therefore, in this paper, pure $ZnBiNbO_5$ with a pyrochlore-type structure was synthesized by a solid-state reaction for the first time. Also, a GaOOH/$ZnBiNbO_5$ composite photocatalyst was constructed to degrade enrofloxacin under illumination in this paper. Characterizations were performed to analyze the properties of the GaOOH/$ZnBiNbO_5$ composite, which included X-ray diffraction (XRD), scanning electron microscopy (SEM), Fourier transform infrared spectroscopy (FT-IR), X-ray photoelectron spectroscopy (XPS), and UV-Visible diffuse reflectance spectroscopy (UV-Vis DRS). In the experiment of degrading enrofloxacin under illumination, the reusability of the GaOOH/$ZnBiNbO_5$ composite was studied and the active radicals in the degradation process were also analyzed. Finally, the superoxide radicals and hydroxyl radicals which were generated in the photocatalytic process were determined by electron paramagnetic resonance (EPR).

Experimental

Synthesis and characterization

The solid-state reaction method was used to synthesize pure $ZnBiNbO_5$, and the typical steps are as follows: (i) according to the theoretical atomic ratio of Zn : Bi : Nb (1 : 1 : 1), ZnO, Bi_2O_3 and Nb_2O_5 (Sinopharm Group Chemical Reagent Co., Ltd., Shanghai, China) were weighed accurately. The purity of the raw materials was 99.99%, and these raw materials were not subjected to further purity treatment. (ii) The three weighed raw materials were ground for 1 h for thorough mixing; then, the mixed powder was pressed into a small column and placed in an alumina crucible (Shenyang Crucible Co., Ltd., Shenyang, China). (iii) The crucible containing the mixed powder was placed in an electric furnace (KSL 1700X, Hefei Kejing Materials Technology Co., Ltd., Hefei, China). The temperature and time of calcination were set to 1100 °C and 25 h, respectively. Finally, the pure $ZnBiNbO_5$ sample was obtained.

The solvothermal method was used to synthesize the GaOOH/$ZnBiNbO_5$ composite, and the synthesis process was as follows: (i) 1.1296 g Ga_2O_3 powder (Aladdin Biochemical Technology Co., Ltd., Shanghai, China) and 2.4762 g pure $ZnBiNbO_5$ were weighed accurately. The purity of the Ga_2O_3 powder was 99.99%, and it was not subjected to further purity treatment. (ii) The weighed powders were placed in a beaker, and 80 ml water and 80 ml absolute ethanol were added. (iii) The above solution was stirred for 30 min at room temperature; then, the solution was transferred into a 200 mL tetrafluoro-lined reactor. (iv) The reactor was placed in an oven and heated at 200 °C for 12 h. (v) After cooling to room temperature, the products were washed several times with water and absolute ethanol and then dried at 60 °C for 12 h. In addition, as a control sample, pure GaOOH was synthesized according to the above process without adding pure $ZnBiNbO_5$.

A powder X-ray diffractometer (XRD, D/MAX-RB, Rigaku Corporation, Japan) with CuKα radiation ($\lambda = 1.54056$) was used to analyze the crystal structure of the GaOOH/$ZnBiNbO_5$ composite. The scan range was set to 10 to 80° and the XRD data were obtained using a step-scan program at 295 K. Scanning electron microscopy - X-ray energy dispersion spectroscopy (SEM-EDS, LEO 1530VP, LEO Corporation, Dresden, Germany) was used to analyze the morphological features of the GaOOH/$ZnBiNbO_5$ composite. X-ray photoelectron spectroscopy (XPS, ESCALABMK-2, VG Scientific Ltd., London, UK) was used to analyze the elemental contents of the GaOOH/$ZnBiNbO_5$ composite. A Fourier transform infrared spectrometer (Nexus, Nicolet Corporation, Madison, WI, USA) with attenuated total reflectance (ATR) mode was used to analyze the main chemical vibrational species of the GaOOH/$ZnBiNbO_5$ composite. A UV-Vis spectrophotometer (UV-2450, Shimadzu Corporation, Kyoto, Japan) was used to analyze the band gap of the GaOOH/$ZnBiNbO_5$ composite. The background material was pure $BaSO_4$ powder.

Photocatalytic activity tests

The degradation of enrofloxacin was selected to evaluate the photocatalytic activity of the GaOOH/$ZnBiNbO_5$ composite. The photocatalytic experiments were performed in a photocatalytic reactor (Xujiang Machine, Nanjing, China) containing optical filters (λ < 400 nm), a mercury lamp (500 W) and a magnetic stirring device. The major emission wavelength of the mercury lamp was 365 nm. Firstly, 50 ml enrofloxacin solution and 0.05 g photocatalyst were placed in a test tube, and the initial concentration of enrofloxacin was set to 10 mg L^{-1}. Then, the tube was placed in the dark for 30 min for dark adsorption. Subsequently, the mercury lamp was turned on for irradiation. During the process of irradiation, 2 mL solution was taken under ultraviolet light for 10 min, 20 min, 30 min, 40 min, and 60 min. The absorbance of enrofloxacin was measured at 276 nm using the UV-visible spectrophotometer (UV-2550, Shimadzu Corporation, Kyoto, Japan). The removal rate of enrofloxacin (D%) was calculated according to the formula: $D\% = (C_0 - C_t)/C_0 \times 100\%$, where C_0 is the initial concentration of enrofloxacin and C_t is the concentration of enrofloxacin at time t. The three-dimensional fluorescence of enrofloxacin was determined by a full-function fluorescence spectrometer (Fluoromax-4, Horiba Scientific). In addition, the active free radicals which were generated during the photocatalytic process were determined by the electron paramagnetic resonance (EPR) method.

Results and discussion

Morphology analysis

The morphologies of $ZnBiNbO_5$, GaOOH and the GaOOH/$ZnBiNbO_5$ composite are displayed in the SEM images shown in Fig. 1(a–c). It can be observed that the as-prepared $ZnBiNbO_5$ presented an irregular particle morphology. Fig. 1(b) displays that the as-prepared GaOOH presented a regular rod morphology with a cracked surface, which may

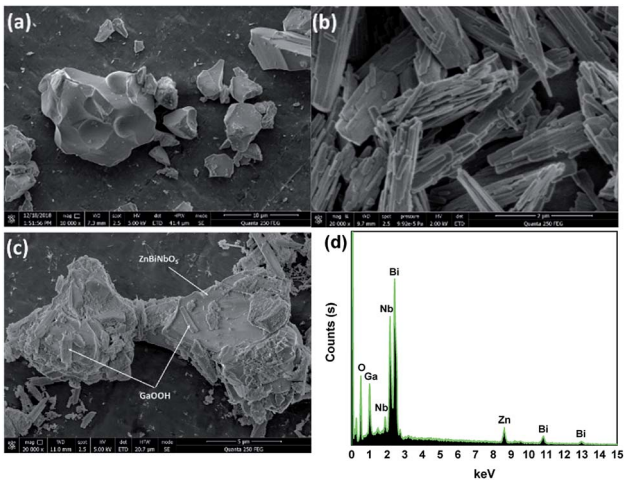

Fig. 1 SEM images of $ZnBiNbO_5$ (a), GaOOH (b), and GaOOH/$ZnBiNbO_5$ (c); EDS pattern of GaOOH/$ZnBiNbO_5$ (d).

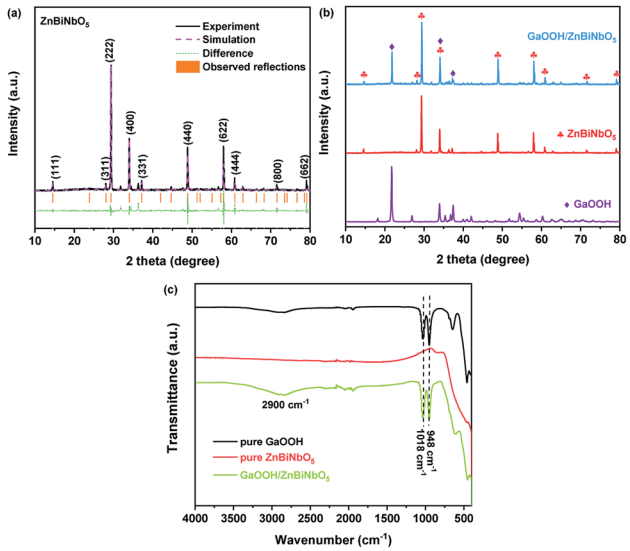

Fig. 2 (a) Pawley refinements of $ZnBiNbO_5$; (b) XRD patterns of $ZnBiNbO_5$, GaOOH and GaOOH/$ZnBiNbO_5$; (c) FT-IR spectra of $ZnBiNbO_5$, GaOOH and GaOOH/$ZnBiNbO_5$.

provide a greater surface area to absorb contaminants. The SEM image of the as-prepared GaOOH/$ZnBiNbO_5$ composite is displayed in Fig. 1(c). It can be clearly seen that the shape of GaOOH in the GaOOH/$ZnBiNbO_5$ composite is random broken rods, which is different from the shape of pure GaOOH. In the GaOOH/$ZnBiNbO_5$ composite, large amounts of GaOOH were dispersed and loaded on the surface of the $ZnBiNbO_5$ particles. This composite structure may provide potential for transfer of photogenerated electrons and photogenerated holes. In addition, the EDS pattern of the GaOOH/$ZnBiNbO_5$ composite is shown in Fig. 1(d); Zn element, Bi element, Nb element, Ga element and O element were all determined successfully.

Structure analysis

The Pawley refinements of $ZnBiNbO_5$ were performed using Materials Studio software to analyze the structure of the as-prepared $ZnBiNbO_5$, and the results are displayed in Fig. 2(a). The observed XRD data of the as-prepared $ZnBiNbO_5$ present good agreement with the theoretical calculated data, which reveals that the as-prepared $ZnBiNbO_5$ was a single phase and had high crystallinity. According to the refinement results, pure $ZnBiNbO_5$ was prepared with a cubic structure in the space group $Fd\bar{3}m$, and the lattice parameters of $ZnBiNbO_5$ are $a = b = c = 10.498767$ Å. The (111), (311), (222), (400), (331), (440), (622), (444), (800) and (662) crystal planes of $ZnBiNbO_5$ are marked in Fig. 2(a). The XRD patterns of $ZnBiNbO_5$, GaOOH and GaOOH/$ZnBiNbO_5$ are displayed in Fig. 2(b). According to our previous research, pure GaOOH crystallizes with an orthorhombic structure in the space group *Pbnm*, and the lattice parameters of GaOOH are $a = 4.509526$ Å, $b = 9.771034$ Å and $c = 2.969284$ Å.[43] It is apparent that the main diffraction peaks of $ZnBiNbO_5$ and GaOOH can both be observed in the XRD pattern of GaOOH/$ZnBiNbO_5$, as shown in Fig. 2(b); this indicates that $ZnBiNbO_5$ was not destroyed by high temperature and high pressure in the solvothermal process and that GaOOH was successfully composited with $ZnBiNbO_5$. In addition, the FT-IR spectra of $ZnBiNbO_5$, GaOOH and GaOOH/$ZnBiNbO_5$ are displayed in Fig. 2(c). A broad peak at 2900 cm^{-1} and two sharp peaks at 1018 cm^{-1} and 948 cm^{-1} are present in the FT-IR spectrum of GaOOH/$ZnBiNbO_5$; all these peaks belong to GaOOH. The sharp peaks at 1018 cm^{-1} and 948 cm^{-1} were attributed to the constitutional Ga–OH bending mode and its overtones, respectively, and the broad peak at 2900 cm^{-1} was attributed to the vibration of O–H in GaOOH.[44,45] Moreover, the relative positions and strengths of the two characteristic peaks at 948 cm^{-1} and 1018 cm^{-1} were related to the shape of the GaOOH.[46]

In order to study the elemental composition and chemical states of the GaOOH/$ZnBiNbO_5$ composite, X-ray photoelectron spectroscopy (XPS) measurements were performed, and the results are displayed in Fig. 3. The high-resolution XPS data of the Zn2p peaks are displayed in Fig. 3(a); the spectrum consists of two peaks at 1025.8 eV and 1048.9 eV, corresponding to the binding energies of $Zn2p_{3/2}$ and $Zn2p_{1/2}$, respectively.[47,48] In Fig. 3(b), the two peaks at 163.0 eV and 164.3 eV can be ascribed to the binding energies of $Bi4f_{7/2}$,[49,50] and the two peaks at 168.5 eV and 169.7 eV can be ascribed to the binding energies of $Bi4f_{5/2}$.[51,52] Simultaneously, the XPS spectrum of Nb3d contains three peaks at 211.7 eV and 212.0 eV (corresponding to $Nb3d_{5/2}$ (ref. 53)) and 214.6 eV (corresponding to $Nb3d_{3/2}$ (ref. 54)), respectively. The XPS spectrum of Ga3d also contains three peaks, and they correspond to the binding energies of $Ga3d_{3/2}$ (19.2 eV)[55] and $Ga3d_{5/2}$ (20.9 eV and 22.5 eV),[56] respectively. There are three peaks at 529.3 eV, 531.0 eV and 532.4 eV in the XPS data of O1s (Fig. 3(e)). The binding energies at 529.3 eV and 531.0 eV belong to the oxygen in the GaOOH/$ZnBiNbO_5$ composite, and the binding energy at 532.4 eV belongs to surface-adsorbed hydroxides.[57]

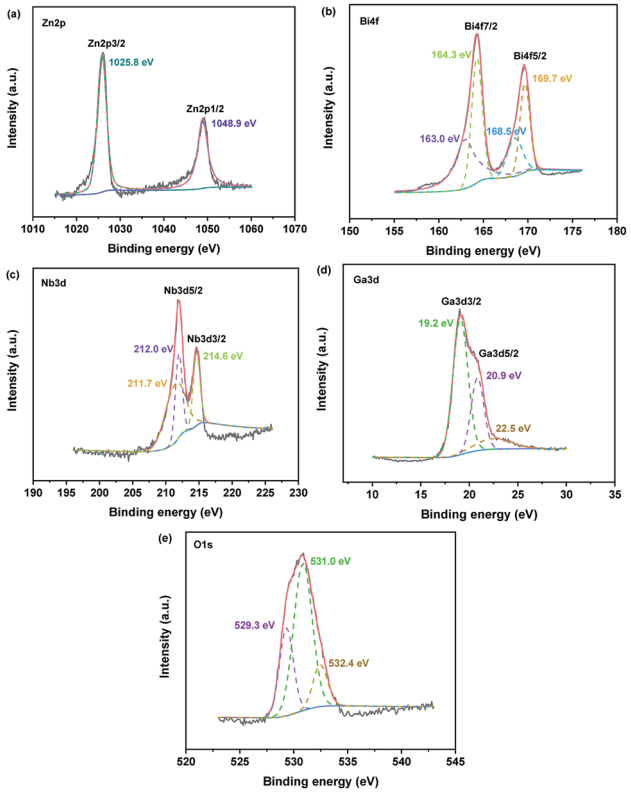

Fig. 3 High-resolution XPS spectra of Zn2p (a), Bi4f (b), Nb3d (c), Ga3d (d) and O1s (e) for GaOOH/$ZnBiNbO_5$.

Optical properties

The UV-Vis diffuse-reflectance spectra of the as-prepared $ZnBiNbO_5$, GaOOH and GaOOH/$ZnBiNbO_5$ are shown in Fig. 4. It can be observed that the absorbance edges of $ZnBiNbO_5$ and GaOOH are 446 nm and 270 nm, respectively.

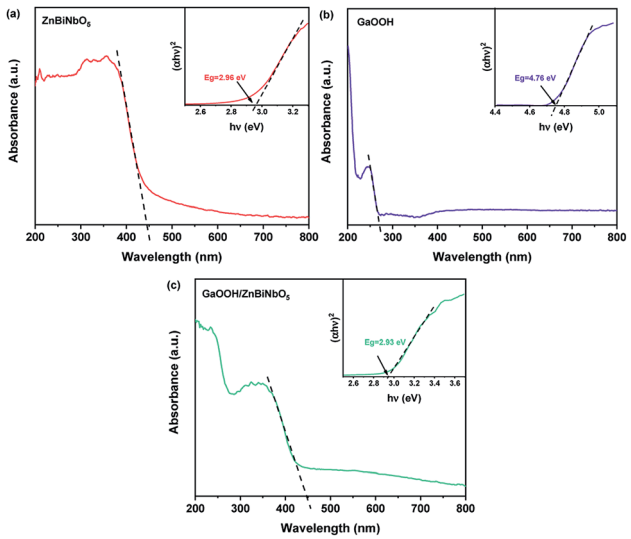

Fig. 4 UV-Vis diffuse-reflectance spectra of $ZnBiNbO_5$ (a), GaOOH (b) and GaOOH/$ZnBiNbO_5$ (c).

After GaOOH was loaded on the surface of $ZnBiNbO_5$, a slight red shift to 450 nm was observed in the absorbance edge of GaOOH/$ZnBiNbO_5$. This phenomenon indicates that the absorption spectra of GaOOH and $ZnBiNbO_5$ were both adjusted by dispersing GaOOH on the surface of $ZnBiNbO_5$. In this paper, we used the Kubelka–Munk transformation method to analyze the band gaps of the samples. The optical absorption near the band edge of the crystalline semiconductors matches the formula $\alpha h\nu = A(h\nu - E_g)^n$,[58,59] where A, E_g, α and n are the proportional constant, band gap, absorption coefficient and light frequency, respectively. According to the above formula, the band gaps of $ZnBiNbO_5$, GaOOH and GaOOH/$ZnBiNbO_5$ were calculated to be 2.96 eV, 4.76 eV and 2.93 eV, respectively, as shown in the inset figures of Fig. 4. A decreased band gap is beneficial for improving photocatalytic activity under solar illumination.

Photocatalytic activity

The photocatalytic activity of the as-prepared GaOOH/$ZnBiNbO_5$ composite was evaluated by photodegradation of enrofloxacin under ultraviolet light irradiation. For comparison, the photocatalytic activities of pure $ZnBiNbO_5$ and pure GaOOH were also investigated. The removal rates of enrofloxacin and the degradation kinetics of enrofloxacin with $ZnBiNbO_5$, GaOOH or GaOOH/$ZnBiNbO_5$ as a photocatalyst are displayed in Fig. 5. As shown in Fig. 5(a), the as-prepared GaOOH/$ZnBiNbO_5$ composite presented good performance for degrading enrofloxacin. After ultraviolet light irradiation for

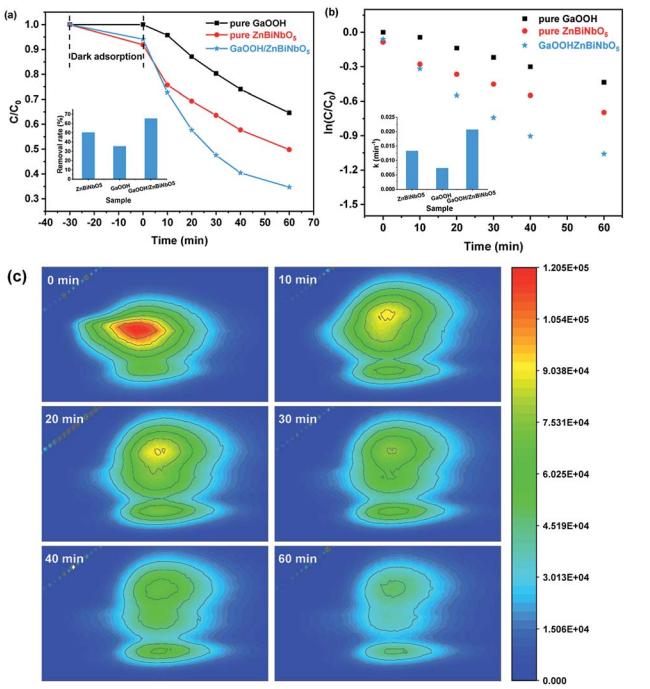

Fig. 5 (a) Removal rates of enrofloxacin and (b) degradation kinetics of enrofloxacin with $ZnBiNbO_5$, GaOOH or GaOOH/$ZnBiNbO_5$ as a photocatalyst; (c) three-dimensional fluorescence change process of enrofloxacin during photocatalytic degradation with GaOOH/$ZnBiNbO_5$ as a photocatalyst.

60 min, the removal rate of enrofloxacin with as-prepared GaOOH/$ZnBiNbO_5$ as a photocatalyst was 65.31%, which was 15.11% higher than that of pure $ZnBiNbO_5$ and 29.29% higher than that of pure GaOOH. The degradation of enrofloxacin can be attributed to a pseudo-first-order kinetics reaction with a simplified Langmuir–Hinshelwood model: $\ln(C/C_0) = -kt$, where k is the pseudo-first-order rate constant and t is the reaction time. When the initial concentration of contaminant is low, this model is generally selected to analyze the photocatalytic degradation kinetics. The degradation kinetics of enrofloxacin with $ZnBiNbO_5$, GaOOH or GaOOH/$ZnBiNbO_5$ as a photocatalyst according to the above formula are shown in Fig. 5(b). The degradation rate of enrofloxacin with GaOOH/$ZnBiNbO_5$ as a photocatalyst was calculated to be 0.02064 min^{-1}, which was 1.56 times that of pure $ZnBiNbO_5$ (0.01326 min^{-1}) and 2.84 times that of pure GaOOH (0.00728 min^{-1}). The photocatalytic activities of both pure $ZnBiNbO_5$ and pure GaOOH were enhanced significantly by loading GaOOH on the surface of $ZnBiNbO_5$. In addition, the three-dimensional fluorescence change process of enrofloxacin during photocatalytic degradation with GaOOH/$ZnBiNbO_5$ as a photocatalyst is displayed in Fig. 5(c). It can be directly observed that as the photocatalytic reaction progressed, the three-dimensional fluorescence center point of enrofloxacin slowly changed from red to light green, indicating that enrofloxacin was gradually degraded.

To evaluate the stability and reusability of the GaOOH/$ZnBiNbO_5$ composite, four rounds of degradation experiments for enrofloxacin under ultraviolet light irradiation with GaOOH/$ZnBiNbO_5$ as a photocatalyst were performed. As shown in Fig. 6(a), as the number of cycles increased, the removal rate of enrofloxacin gradually decreased. From the first round to the fourth round, the removal rates of enrofloxacin were 65.31%, 58.97%, 51.92% and 48.82%, respectively. After four rounds of circulation, the enrofloxacin removal rate was decreased by 16.49%. In addition, the removal rates of enrofloxacin with different initial pH values using GaOOH/$ZnBiNbO_5$ as a photocatalyst were studied to explore the adaptability of GaOOH/$ZnBiNbO_5$ to the pH of the pollutant solution, and the results are displayed in Fig. 6(b). It can be seen that when the initial pH values of the enrofloxacin solution were 3, 5, 9 and 11, the removal rates of enrofloxacin were all lower than the removal rate at an initial pH of 7; this indicates that neither acidic nor basic conditions are conducive to the degradation of enrofloxacin. It is worth noting that the removal rate of enrofloxacin under acidic conditions was lower than that of enrofloxacin under alkaline conditions. A possible reason is that the abundant hydroxide ions in the solution under alkaline conditions can be converted into hydroxyl radicals to participate in the photocatalytic reaction. Moreover, the effects of different cations and anions on the degradation of enrofloxacin using GaOOH/$ZnBiNbO_5$ as a photocatalyst were determined. As shown in Fig. 6(c) and (d), Al^{3+}, Fe^{3+}, Cu^{2+}, CO_3^{2-} and SO_4^{2-} had almost no effect on the degradation of enrofloxacin. However, NO_3^- had an inhibitory effect on the degradation of enrofloxacin; the addition of NO_3^- decreased the removal rate of enrofloxacin by 10.95%. Overall, the as-prepared GaOOH/$ZnBiNbO_5$ has strong potential for adaptation to actual wastewater and is expected to be further applied to the degradation of enrofloxacin pollutants in actual wastewater.

The removal of enrofloxacin with the addition of different radical scavengers using GaOOH/$ZnBiNbO_5$ as a photocatalyst was studied to analyze the possible active species in the photocatalytic degradation process. The radical scavengers used herein were benzoquinone (BQ), ethylenediaminetetraacetic acid (EDTA) and *tert*-butanol (TBA), which are scavengers for $\cdot O_2^-$, h^+ and $\cdot OH$, respectively. The addition amounts of BQ,

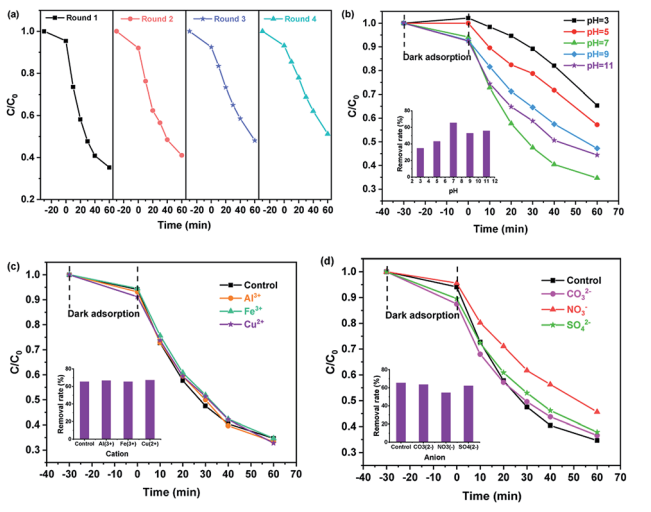

Fig. 6 (a) Cycle degradation of enrofloxacin with an initial pH of 7 using GaOOH/$ZnBiNbO_5$ as a photocatalyst; (b) removal rate of enrofloxacin with different initial pH values using GaOOH/$ZnBiNbO_5$ as a photocatalyst; the effects of different cations (c) and anions (d) on the degradation of enrofloxacin using GaOOH/$ZnBiNbO_5$ as a photocatalyst.

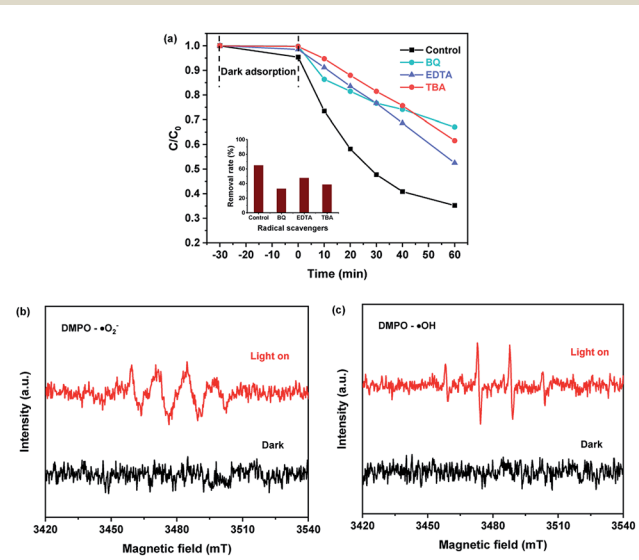

Fig. 7 (a) Removal of enrofloxacin with the addition of different radical scavengers using GaOOH/$ZnBiNbO_5$ as a photocatalyst; DMPO spin-trapping EPR spectra of GaOOH/$ZnBiNbO_5$ in a methanol dispersion for DMPO–$\cdot O_2^-$ (b) and in an aqueous dispersion for DMPO–$\cdot$OH (c).

EDTA and TBA were 1 mL, and the concentrations of BQ, EDTA and TBA were 0.15 mmol L^{-1}. It can be found in Fig. 7(a) that the addition of BQ, EDTA and TBA all deceased the removal rate of enrofloxacin. Compared with the control group, the removal rate of enrofloxacin declined by 31.88%, 17.31% and 26.33%, respectively, when BQ, EDTA and TBA were added. Therefore, it can be concluded that the order of the contribution of the free radicals to the photocatalytic process is as follows: $\cdot O_2^-$ > ·OH > h^+.

$$h^+ + OH^- \rightarrow \cdot OH \quad (1)$$

$$h^+ + H_2O \rightarrow \cdot OH + H^+ \quad (2)$$

$$e^- + O_2 \rightarrow \cdot O_2^- \quad (3)$$

$$\cdot O_2^- + H^+ \rightarrow \cdot O_2H \quad (4)$$

The $\cdot O_2^-$ and ·OH radicals are produced in the photocatalytic process, as shown in eqn (1)–(4). In alkaline solution, a large amount of OH^- promotes the formation of ·OH (eqn (1)) and inhibits the consumption of $\cdot O_2^-$ (eqn (4)). However, in acidic solution, a large amount of H^+ inhibits the formation of ·OH (eqn (2)) and promotes the consumption of $\cdot O_2^-$ (eqn (4)). This is why the removal rate of enrofloxacin under acidic conditions is lower than that of enrofloxacin under alkaline conditions.

To further confirm the presence of $\cdot O_2^-$ and ·OH, EPR characterization was carried out using 5,5-dimethyl-1-pyrroline N-oxide (DMPO) as a spin to trap the active radicals in the system for detection. As shown in Fig. 7(b) and (c), no signals relevant to DMPO/$\cdot O_2^-$ adducts or DMPO/·OH adducts were detected under dark conditions. However, after ultraviolet light irradiation, signals were presented. It can be observed clearly in Fig. 7(b) that there was a signal of four peaks with nearly the same intensity, corresponding to the DMPO/$\cdot O_2^-$ adduct. Similarly, in Fig. 7(c), a typical four-line signal with a relative intensity ratio close to 1 : 2 : 2 : 1 could be observed, which is a characteristic signal of the DMPO/·OH adduct.[60] Therefore, $\cdot O_2^-$ and ·OH were actually produced during the photocatalytic process, which is consistent with the free radical scavenging experiment results.

Conclusions

In summary, we prepared a GaOOH/$ZnBiNbO_5$ composite by loading GaOOH rods on the surface of $ZnBiNbO_5$ particles; $ZnBiNbO_5$ is a novel photocatalyst that was prepared in this paper for the first time. The morphology, structure, optical properties and photocatalytic activity of GaOOH/$ZnBiNbO_5$ were all studied in this paper. According to SEM images, GaOOH was successfully dispersed on the surface of $ZnBiNbO_5$ to construct a composite structure. Using the Pawley method, the XRD data of pure $ZnBiNbO_5$ were refined; the refinement results showed that the novel as-prepared $ZnBiNbO_5$ had a cubic structure and a space group of $Fd\bar{3}m$, and the lattice parameters of $ZnBiNbO_5$ were $a = b = c = 10.498767$ Å. The main diffraction peaks of both $ZnBiNbO_5$ and GaOOH were observed in the XRD pattern of the GaOOH/$ZnBiNbO_5$ composite. In addition, UV-Vis DRS characterization was carried out to analyse the optical properties of the samples, and the results showed that there was a red-shift of the absorbance edge of GaOOH/$ZnBiNbO_5$ compared with those of pure $ZnBiNbO_5$ and pure GaOOH. The band gaps of $ZnBiNbO_5$, GaOOH and GaOOH/$ZnBiNbO_5$ were calculated to be 2.96 eV, 4.76 eV and 2.93 eV, respectively. Finally, the photocatalytic activity of GaOOH/$ZnBiNbO_5$ was explored by degrading enrofloxacin under ultraviolet light irradiation. The as-prepared GaOOH/$ZnBiNbO_5$ presented much higher photocatalytic performance than pure $ZnBiNbO_5$ or pure GaOOH. After ultraviolet light irradiation for 60 min, the removal rate of enrofloxacin with GaOOH/$ZnBiNbO_5$ as a photocatalyst was 15.11% higher than that of pure $ZnBiNbO_5$ and was 29.29% higher than that of pure GaOOH. According to the free radical scavenging experiment results and the EPR characterization, the contribution of the free radicals in the photocatalytic process was as follows: $\cdot O_2^-$ > ·OH > h^+. Overall, the construction of the GaOOH/$ZnBiNbO_5$ composite enhanced the photocatalytic performance of both pure $ZnBiNbO_5$ and pure GaOOH, resulting in more effective removal of enrofloxacin pollutants from water and purification of the water.

Conflicts of interest

There are no conflicts to declare.

Acknowledgements

This work was supported by a grant from the China-Israel Joint Research Program in Water Technology and Renewable Energy (No. 5). This work was supported by a grant from the Technological Supporting Foundation of Jiangsu Province (No. BE2009144). This work was supported by the National Natural Science Foundation of China (No. 20877040).

References

1 A. M. Diogo Alexandrino, A. P. Mucha, C. M. R. Almeida, W. Gao, Z. J. Jia and M. F. Carvalho, *Sci. Total Environ.*, 2017, **581–582**, 359–368.
2 T. V. Boeckel, S. Gandra, A. Ashok, Q. Caudron, B. T. Grenfell, S. A. Levin and R. Laxminarayan, *Lancet Infect. Dis.*, 2014, **14**(8), 742–750.
3 H. S. Qian, P. Gunawan, Y. X. Zhang, G. F. Lin, J. W. Zheng and R. Xu, *Cryst. Growth Des.*, 2008, **8**, 1282.
4 G. L. Cromwell, *Anim. Biotechnol.*, 2002, **13**(1), 7–27.
5 X. Li, W. Zheng, M. L. Machesky, S. R. Yates and M. Katterhenry, *J. Agric. Food Chem.*, 2011, **59**(18), 10176–10181.
6 M. S. Fortunato, N. P. F. Abril, M. Martinefski, V. Tripodi, M. Papalia, M. Rádice, G. Gutkind, A. Gallego and S. E. Korol, *Environ. Technol.*, 2016, **37**(20), 2617–2626.
7 M. L. Loke, F. Ingerslev, B. Halling Sørensen and J. Tjørnelund, *Chemosphere*, 2000, **40**(7), 759–765.

8 R. P. Tasho and J. Y. Cho, *Sci. Total Environ.*, 2016, **563–564**, 366–376.
9 J. Corcoran, M. J. Winter and C. R. Tyler, *Crit. Rev. Toxicol.*, 2010, **40**(4), 287–304.
10 H. K. Allen, J. Donato, H. H. Wang, K. A. Cloud-Hansen, J. Davies and J. Handelsman, *Nat. Rev. Microbiol.*, 2010, **8**, 251–259.
11 V. M. F. Frade, M. Dias, A. C. S. C. Teixeira and M. S. A. Palma, *Braz. J. Pharm. Sci.*, 2014, **50**(1), 41–54.
12 X. Van Doorslaer, J. Dewulf, H. Van Langenhove and K. Demeestere, *Sci. Total Environ.*, 2014, **500–501**, 250–269.
13 W. Ben, X. Pan and Z. Qiang, *Environ. Sci.: Processes Impacts*, 2013, **15**, 870–875.
14 M. Ferri, E. Ranucci, P. Romagnoli and V. Giaccone, *Crit. Rev. Food Sci. Nutr.*, 2017, **57**, 2857–2876.
15 X. Huang, C. Liu, K. Li, F. Liu, D. Liao, L. Liu, G. Zhu and J. Liao, *Environ. Sci. Pollut. Res.*, 2013, **20**(12), 9066–9074.
16 J. Xu, Y. Xu, H. Wang, C. Guo, H. Qiu, Y. He, Y. Zhang, X. Li and W. Meng, *Chemosphere*, 2015, **119**, 1379–1385.
17 G. K. C. Low, S. R. Mcevoy and R. W. Matthews, *Environ. Sci. Technol.*, 1991, **25**, 460–467.
18 J. Matos, J. Laine and J. M. Herrmann, *J. Catal.*, 2001, **200**, 10–20.
19 F. Lu, W. P. Cai and Y. G. Zhang, *Adv. Funct. Mater.*, 2008, **18**, 1047–1056.
20 W. Zhao, W. H. Ma, C. C. Chen, J. C. Zhao and Z. G. Shuai, *J. Am. Chem. Soc.*, 2004, **126**, 4782–4783.
21 A. A. Khodja, B. Lavedrine, C. Richard and T. Sehili, *Int. J. Photoenergy*, 2002, **4**, 147–151.
22 A. A. Murashkina, P. D. Murzin, A. V. Rudakova, V. K. Ryabchuk, A. V. Emeline and D. W. Bahnemann, *J. Phys. Chem. C*, 2015, **119**, 24695–24703.
23 D. Eder, M. Motta and A. H. Windle, *Nanotechnology*, 2009, **20**, 055602.
24 S. K. Biswas and J. O. Baeg, *Int. J. Hydrogen Energy*, 2013, **38**, 14451–14457.
25 S. Anandan, T. N. Rao, R. Gopalan and Y. Ikuma, *J. Nanosci. Nanotechnol.*, 2014, **14**, 3181–3186.
26 K. Dai, J. L. Lv, L. H. Lu, C. H. Liang, L. Geng and G. P. Zhu, *Mater. Chem. Phys.*, 2016, **177**, 529–537.
27 T. P. Xie, C. L. Liu, L. J. Xu, J. Yang and W. Zhou, *J. Phys. Chem. C*, 2013, **117**, 24601–24610.
28 X. F. Wang, H. M. Hu, S. H. Chen, K. H. Zhang, J. Zhang, W. S. Zou and R. X. Wang, *Mater. Chem. Phys.*, 2015, **158**, 67–73.
29 X. Zong, J. F. Han, G. J. Ma, H. J. Yan, G. P. Wu and C. Li, *J. Phys. Chem. C*, 2011, **115**, 12202–12208.
30 Y. H. Hsu, A. T. Nguyen, Y. H. Chiu, J. M. Li and Y. J. Hsu, *Appl. Catal., B*, 2016, **185**, 133–140.
31 X. Zong, H. J. Yan, G. P. Wu, G. J. Ma, F. Y. Wen, L. Wang and C. Li, *J. Am. Chem. Soc.*, 2008, **130**, 7176–7177.
32 M. Pirhashemi and A. Habibi-Yangjeh, *J. Colloid Interface Sci.*, 2016, **474**, 103–113.
33 X. F. Chen, J. Zhang, Y. N. Huo and H. X. Li, *Chin. J. Catal.*, 2013, **34**, 949–955.
34 H. J. Lu, L. L. Xu, B. Wei, M. Y. Zhang, H. Gao and W. J. Sun, *Appl. Surf. Sci.*, 2014, **303**, 360–366.
35 J. Cao, B. Y. Xu, H. L. Lin, B. D. Luo and S. F. Chen, *Catal. Commun.*, 2012, **26**, 204–208.
36 A. L. M. Reddy, S. R. Gowda, M. M. Shaijumon and P. M. Ajayan, *Adv. Mater.*, 2012, **24**(37), 5045–5064.
37 J. L. Shi, *Chem. Rev.*, 2013, **113**(3), 2139–2181.
38 Z. G. Zou and H. Arakawa, *J. Photochem. Photobiol., A*, 2003, **158**, 145–162.
39 B. Cui, H. Lin, Y. Z. Li, J. B. Li, P. Sun and X. C. Zhao, *J. Phys. Chem. C*, 2009, **32**, 14083–14087.
40 J. F. Luan, S. Wang, K. Ma, Y. M. Li and B. C. Pan, *J. Phys. Chem. C*, 2010, **114**, 9398–9407.
41 M. Sun, D. Li, W. Zhang, X. Fu, Y. Shao, W. Li, G. Xiao and Y. He, *Nanotechnology*, 2010, **21**, 355601.
42 J. Sato, H. Kobayyashi and Y. Inoue, *J. Phys. Chem. B*, 2003, **107**, 7970–7975.
43 P. Q. Huang and J. F. Luan, *RSC Adv.*, 2019, **9**, 19930–19939.
44 G. G. Li, C. Peng, C. X. Li, P. P. Yang, Z. Y. Hou, Y. Fan, Z. Y. Cheng and J. Lin, *Inorg. Chem.*, 2010, **49**, 1449–1457.
45 X. H. Liu, G. Z. Qiu, Y. Zhao, N. Zhang and R. Yi, *J. Alloys Compd.*, 2007, **439**, 275–278.
46 S. Krehula, M. Ristíc, S. Kubuki, Y. Iida, M. Fabían and S. Musíc, *J. Alloys Compd.*, 2015, **620**, 217–227.
47 L. G. Mar, P. Y. Timbrell and R. N. Lamb, *Thin Solid Films*, 1993, **223**, 341–347.
48 R. Strohmeier, *Surf. Sci. Spectra*, 1994, **3**, 141–146.
49 F. M. Ismail and Z. M. Hanafi, *Z. Phys. Chem.*, 1986, **267**, 667–672.
50 W. E. Morgan, W. J. Stec and J. R. Van Wazer, *Inorg. Chem.*, 1973, **12**, 953–955.
51 A. R. H. F. Ettema and C. Haas, *J. Phys.: Condens. Matter*, 1993, **5**, 3817–3826.
52 K. Shukla, A. M. Kannan, M. S. Hegde and J. Gopalakrishnan, *J. Power Sources*, 1991, **35**, 163–173.
53 M. A. B. Gomes, L. O. d. S. Bulhoes, S. C. de Castro and A. J. Damiao, *J. Electrochem. Soc.*, 1990, **137**, 3067.
54 V. L. Teixeira da Silva, M. Schmal and T. Oyama, *J. Solid State Chem.*, 1996, **123**, 168–182.
55 J. Hwang, P. Pianetta, C. K. Shih, W. E. Spicer, Y. C. Pao and J. S. Harris Jr, *Appl. Phys. Lett.*, 1987, **51**, 1632–1633.
56 H. Iwakuro, C. Tatsuyama and S. Ichimura, *Jpn. J. Appl. Phys.*, 1982, **21**, 94–99.
57 F. Conrad, M. Bauer, D. Sheptyakov, S. Weyeneth, D. Jaeger, K. Hametner, P. E. Car, J. Patscheider, D. Günther and G. R. Patzke, *RSC Adv.*, 2012, **2**, 3076–3082.
58 J. Tauc, R. Grigorov and A. Vancu, *Phys. Status Solidi*, 1966, **15**, 627–637.
59 M. A. Butler, *J. Appl. Phys.*, 1977, **48**, 1914–1920.
60 Y. Liu, S. Yu, Z. Y. Zhao, F. Dong, X. A. Dong and Y. Zhou, *J. Phys. Chem. C*, 2017, **121**(22), 12168–12177.